PHYSICAL REVIEW A VOLUME 32, NUMBER 1 JULY 1985

Statistical properties of the quantized energy spectrum of a Hamiltonian system with classically regular and chaotic trajectories: A numerical study of level-spacing distributions for two-dimensional coupled Morse-oscillator systems

Toshitaka Terasaka
Department of Chemistry, Ibaraki University, Mito, Ibaraki 310, Japan

Toshiki Matsushita
Department of Chemistry, Faculty of Science and Technology, Keio University, Hiyoshi 3-14-1, Yokohama 223, Japan
(Received 23 August 1984)

A quantification of the degree of classical chaos manifested in the quantized energy spectra of two—degree-of-freedom coupled Morse-oscillator systems with sufficiently dense energy levels is attempted by use of Brody's repulsion parameter which characterizes his nearest-neighbor level-spacing distribution function. A close relationship is established numerically between the mass-ratio dependence of the Brody parameter and that of the relative area of the chaotic regions on the Poincaré surfaces of section in the corresponding classical system. It is shown that in the strong-coupling limit the distribution appears to tend to the Mehta-Gaudin distribution from the random matrix theory, suggesting that in this limit it is almost impossible to distinguish between the quantized version of the classical K system and those of other systems with a fairly small number of regular trajectories. The present analysis also demonstrates that the Brody parameter serves as a useful indicator for measuring the degree of mode coupling and for detecting an isolated local mode in the system.

I. INTRODUCTION

The statistical analysis of energy spectra of complicated systems has a long history, notably in the field of nuclear spectroscopy, in the form of statistical or random matrix theory of spectra, and a large amount of theoretical and experimental work has resulted.[1–4] Recently, the analysis has attracted a renewed and increasing interest in another field of research, in connection with the statistical or random properties of quantum spectra of nonlinear systems whose classical motions exhibit chaotic behavior.[5–14] So far, the theory has mainly been applied to simple K systems such as the stadium system[5,6] or Sinai's billiard system[7,13] whose ergodicity in the classical limit has been rigorously proved. The results obtained have shown that the nearest-neighbor level-spacing distributions are sufficiently close to the Wigner[3] or, more precisely, to the Mehta-Gaudin[15,16] distribution derived from the Gaussian orthogonal ensemble (GOE) of random matrices. Along with the recent rise in interest, stimulated by advances in laser technology, in high-lying vibrational excited states of polyatomic molecules, the applications of the theory are now being directed toward realistic systems.[17–20]

In a previous paper[12] (hereafter referred to as I), in connection with classical chaos also treated previously in another paper[21] (referred to as II), we obtained quantized energy spectra and constructed the associated nearest-neighbor level-spacing distributions for a family of two-dimensional Morse-oscillator systems interacting through off-diagonal kinetic-energy terms. In I, although we found, as a function of mass ratio δ, a certain parallel relationship between the degree of classical chaos and the curve profiles of nearest-neighbor level-spacing distributions, we did not attempt to carry out any test of goodness of fit of the obtained histograms to particular known distribution curves, because of rather large statistical fluctuations caused by the small number of energy levels.

The purpose of the present paper, accordingly, is to compute the energy spectrum by increasing the number of energy levels and to quantify the degree of chaotic development reflected in the quantum energy spectrum from a rather phenomenological statistical standpoint, by employing the repulsion parameter introduced by Brody[22] (hereafter called the Brody parameter) as a generalization of the Wigner distribution.

Throughout our series of studies, including the present one, we have used triatomic model systems under the two—degree-of-freedom approximation given by freezing the bending vibrational mode. Triatomic systems have three or four vibrational degrees of freedom according to whether they are bent or linear. Hence, the increase in the number of vibrational energy levels below the dissociation threshold should, in principle, be brought about by incorporating the remaining bending vibrational mode(s) neglected in previous treatments. At the present stage, however, it is almost impossible to carry out a systematic, three-dimensional treatment including the bending mode since a three-dimensional model potential function, applicable universally in the same way as the Morse function for the one-dimensional case, is not known particularly for the dissociation energy range. Therefore, in this paper we adopt an alternative approach of increasing the number of energy levels by raising the values of masses, from those of ordinary molecular systems up to sufficiently

large values to allow us to determine the two-level correlation measures with a much higher accuracy. As can be easily noticed, this procedure is equivalent to making the system closer to the semiclassical limit by employing a smaller $\hbar$. Although the computational results of such a substitution cannot be compared directly with those of actual molecular systems, the procedure is expected to serve sufficiently well for the main objective of the present study, that is, an understanding of the statistical properties of the quantum energy spectra of Hamiltonian systems with strong coupling among different degrees of freedom in the limit of sufficiently small but finite $\hbar$.

The outline of this paper is as follows. In Sec. II we provide the model Hamiltonian and the associated matrix elements for the present analysis, as well as the definition of the Brody distribution function which serves as an interpolation formula between the Poisson distribution in the zero-coupling limit and the Wigner distribution in the strong-coupling limit. In Sec. IV we present a relationship between the mass ratio and the Brody parameter and show that in fact a stong correlation exists between the mass ratio dependence of the Brody parameter and that of the relative chaotic area on the Poincaré sections in the corresponding classical system. Section IV is devoted to some detailed analysis of the origin of such a classical-quantum correspondence which holds over a wide range of δ values, with the aid of Poincaré sections at certain typical mass ratios and energy values. In Sec. V a summary and concluding remarks are presented.

II. MODEL SYSTEM AND THE BRODY DISTRIBUTION FUNCTION

The model Hamiltonian and associated matrix elements for the present analysis are given in I.[23] However, in order to make this paper self-contained and for the convenience of the discussion below, we present them briefly, together with the definition of the Brody distribution function. The quantum Hamiltonian of a pair of identical Morse oscillators coupled via an off-diagonal kinetic-energy term is written as

$$H=H_1+H_2+H_{12} , \tag{1}$$

with

$$H_i=-(\hbar^2/2\tilde{m}_i)\partial^2/\partial r_i^2+V_i(r_i), \quad i=1,2 \tag{2}$$

$$H_{12}=\hbar^2\mu_2(\partial/\partial r_1)(\partial/\partial r_2) , \tag{3}$$

$$\tilde{m}_i=(\mu_1+\mu_2)^{-1}, \quad \mu_i=m_i^{-1} \tag{4}$$

$$V_i(r_i)=D_i[\exp(-a_i r_i)-1]^2, \quad i=1,2 \tag{5}$$

where H_i $(i=1,2)$ are the Hamiltonians of the Morse oscillators corresponding to the two adjacent bonds symmetrically located with respect to the central atom having mass m_2, H_{12} is the interaction Hamiltonian between these two bonds representing the so-called kinetic coupling, and r_i $(i=1,2)$ are the displacements of the ith bonds from their equilibrium positions. In Eq. (4), μ_1 and μ_2 are the reciprocals of the masses of the two end and central atoms, respectively, and $\tilde{m}$ $(i=1,2)$ denote the reduced masses of the two identical adjacent Morse oscillators. $V_i(r_i)$ defined in Eq. (5) are the Morse potential functions for the ith bond, and the parameters D_i and a_i are the dissociation energy and scaling parameters related to the force constants of the associated bonds.

The eigenfunctions of the coupled oscillator system, Eq. (1), are approximated in terms of a linear combination of the following product basis constructed from the two Morse-oscillator eigenfunctions:

$$|v_1 v_2^{\pm}>=2^{-1/2}[\phi_{v_1}(r_1)\phi_{v_2}(r_2)\pm\phi_{v_1}(r_2)\phi_{v_2}(r_1)] , \tag{6}$$

with

$$\phi_v(r)=N_v x^{k-v-1/2}\exp(-x/2)L_v^{2k-2v-1}(x) , \quad 0\le v\le[k-\tfrac{1}{2}] \tag{7}$$

$$N_v=\{[a(2k-2v-1)v!]/\Gamma(2k-v)\}^{1/2} , \tag{8}$$

$$x=2k\exp(-ar) , \tag{9}$$

$$k=(2\tilde{m}D)^{1/2}/(a\hbar) , \tag{10}$$

where a combination of $+$ or $-$ sign corresponds to a symmetrized or antisymmetrized basis function, respectively, and $L_v^{2k-2v-1}(x)$ is an associated Laguerre polynomial, $[k-\frac{1}{2}]$ denotes a maximum integer not exceeding the real number $k-\frac{1}{2}$, and v_1 and v_2 are the vibrational quantum numbers of the bond modes 1 and 2, respectively. In Eqs. (7)—(10) we have suppressed the subscripts $i(=1,2)$ of r, x, v, k, a, $\tilde{m}$, and D for notational simplicity. With the use of the basis given in Eq. (6), the matrix elements of the Hamiltonian equation (1) are expressed as

$$\langle v_1' v_2'^{+}|H|v_1 v_2^{+}\rangle=H^{+}_{v_1' v_2';v_1 v_2}=H_{v_1' v_2';v_1 v_2}+H_{v_1' v_2';v_2 v_1} , \tag{11}$$

$$\langle v_1' v_2'^{-}|H|v_1 v_2^{-}\rangle=H^{-}_{v_1' v_2';v_1 v_2}=H_{v_1' v_2';v_1 v_2}-H_{v_1' v_2';v_2 v_1} , \tag{12}$$

with

$$H_{v_1' v_2';v_1 v_2}=\delta_{v_1' v_1}\delta_{v_2' v_2}(e_{v_1}+e_{v_2}) +\hbar^2\mu_2\langle v_1'|(d/dr_1)|v_1\rangle\langle v_2'|(d/dr_2)|v_2\rangle , \tag{13}$$

$$e_{v_i}=D_i[2(v_i+\tfrac{1}{2})/k_i-(v_i+\tfrac{1}{2})^2/k_i^2] , \tag{14}$$

$$\langle v_i'|(d/dr_i)|v_i\rangle=\int\phi_{v_i'}(r_i)(d/dr_i)\phi_{v_i}(r_i)dr_i \tag{15}$$

$$=\begin{cases} N_{v_i'}N_{v_i}(-1)^{v_i'-v_i}\Gamma(2k-v_i')/2v_i! \\ \text{for } v_i'\neq v_i , \\ 0 \text{ for } v_i'=v_i, \quad i=1,2 \end{cases} \tag{16}$$

where the $+$ and $-$ signs in Eqs. (11) and (12) stand for *gerade* (hereafter abbreviated to *g*) and *ungerade* (similarly abbreviated to *u*) eigenstates, respectively, and, in particular, e_{v_i} given by Eq. (14) corresponds to the vibrational en-

ergy in the v_ith vibrational quantum state of the ith Morse oscillator in isolation.

As seen from the form of the Hamiltonian equation (1), in the present model four degrees of freedom, including rotational ones, are neglected. At the present stage it is not clear to what extent the exclusion of these degrees of freedom can be justified for the higher-energy region in which we are interested. Clearly, such a neglect of the other degrees of freedom of the system leads to a decrease in the number of energy levels and lowers the reliability of a statistical treatment. As noted in the Introduction, this potentially unfavorable effect, particularly the neglect of the bending vibrational mode, is to some extent (at least in the sense of the statistical treatment) compensated for by increasing masses in the system. However, in order to effect a correspondence with classical analysis, this has to be done in such a way that the mass ratio δ remains unchanged, since that ratio is one of the two system parameters in the corresponding classical system. This is actually achieved by increasing only the mass of central atom; namely from the definition of the modified mass ratio $\delta=(1+\mu_1/\mu_2)^{-1}$, the dimensionless parameter k, Eq. (10), which provides the maximum vibrational quantum number below the dissociation threshold under condition $0\le v\le[k-\frac{1}{2}]$ in Eq. (7), is rewritten as

$$k=(2\tilde{m}D)^{1/2}/(a\hbar)=[(2\delta D)/\mu_2]^{1/2}/(a\hbar) .$$

From this expression we see that only the mass of the central atom has to be varied. Actually, in our calculation, the largest value of m_2 has been taken to be 1370 (in units of atomic weight) at $\delta=0.01$, the smallest δ value. This somewhat artificial procedure, however, is considered to reproduce qualitative features of the level-structure in an actual physical situation to a considerable extent, as long as the coupling between the stretching and bending vibrational modes in higher-energy region is strong enough to be comparable to that between the two stretching modes.

We now present the difinition of the Brody distribution function employed for the analysis of the nearest-neighbor level spacings in the later sections. The Brody distribution function, characterized by the parameter β, may be written as

$$P_\beta(z)=Az^\beta\exp(-\alpha z^{1+\beta}),\quad z=s/\bar{s} \tag{17}$$

with

$$A=(1+\beta)\alpha,\quad \alpha=[\Gamma((2+\beta)/(1+\beta))/\bar{s}]^{1+\beta} , \tag{18}$$

where s is the nearest-neighbor level spacing and $\bar{s}$ is the mean spacing averaged over the energy interval under consideration, and the parameters A and α given by Eq. (18) are determined from the condition that both the average of z and the area under the curve must be equal to unity. The value of parameter β is found by a nonlinear least-squares fit to the given histograms. Since the distribution function (17) was introduced as an interpolation formula, it tends as $\beta\to 0$ to the Poisson distribution

$$P_p(z)=(1/\bar{s})\exp(-z) ,$$

and, as $\beta\to 1$ to the Wigner distribution,

$$P_w(z)=\frac{\pi z}{2\bar{s}}\exp(-\pi z^2/4) .$$

It should be noted that the nearest-neighbor level-spacing distributions for the GOE derived by Mehta and Gaudin correspond approximately to the Brody distribution with $\beta=0.953$, in contrast to the Wigner distribution with $\beta=1.0$.[1] In later sections our results are discussed with reference to the Mehta-Guadin distribution rather than to the Wigner distribution, since the latter could be regarded as a close, first approximation to the former.

As stated above, the Brody distribution function is not derived by a standard procedure on the basis of a particular random matrix ensemble. Consequently, although in the next section the existence of a certain approximate functional relation could be suggested between the Brody parameter and an averaged fraction of chaotic regions in Poincaré sections at different energies, in this analysis we use this distribution function as being empirically effective in abstracting the essential and major part of the mode coupling, and we expect that naturally another distribution function in a different functional form could be conceived and constructed.[24]

III. QUANTUM LEVEL-SPACING DISTRIBUTIONS AND THEIR MASS RATIO DEPENDENCE

In this section we present quantum energy spectra calculated on the basis of the model Hamiltonian described in the preceding section and the associated nearest-neighbor level-spacing distributions using the Brody distribution function. Our greatest concern in this analysis is to find out whether or not the Brody parameter characterizing the level-spacing distributions exhibits, with the variation of mass ratio δ, the same type of oscillatory behavior as in regular-chaotic area ratios on the Poincaré surfaces of section of the corresponding classical systems.[21] In the present calculations of energy levels, the same set of parameter values as in I ($a=3.1$ Å and $D=5.453$ eV, which corresponds to the dissociation energy of the CO_2 molecule) are employed, except that the masses of central atoms are increased so that the maximum vibrational quantum number below the dissociation threshold of the Morse oscillator for each bond is kept to be 61 throughout all the δ values considered. In order to attain five-decimal-place accuracy on the average (in units of dissociation energy), 1891- and 1830-dimensional matrices for the g and u states, respectively, obtained from all combinations of the two vibrational quantum numbers v_1 and v_2, are diagonalized, and approximately 430 and 410 eigenvalues are obtained for the respective states. From the check of convergence conducted by varying the dimensions of the matrices, a number of eigenvalues in the range $\sim 0.9\le E\le 1.0$ (hereafter, energy is expressed in units of the dissociation energy D) are found to have four-decimal-place accuracy. For example, at $\delta=0.5$, 26 eigenvalues for 1700-dimensional and 7 for 1750-dimensional matrices have turned out to have the lower accuracy, and 10 out of these 26 and 1 out of 7 have been comparable to the smallest value of the level spacings. Consequently, the accuracy of eigenvalues at higher energies near the dissociation threshold is expected to be

somewhat lower than that in lower-energy regions. However, this poorer convergence observed near the dissociation threshold is considered not to have a serious effect on the overall curve profiles of the level-spacing distributions since the inaccuracy of a small number of eigenvalues is smoothed by the statistical procedure in deriving the distribution curves. In fact, in the convergence check it is found that the change in value of the Brody parameter $\Delta\beta$ between the 1891- and the 1600-dimensional cases is ~ 0.01 for the energy range $0.5 \leq E \leq 1.0$ at several δ values. As shown below in Fig. 6, a much more serious convergence problem is caused by the fact that there are not enough levels to construct the distribution curves accurately.

Although the presentation of complete energy-level diagrams of the present model system is not our primary concern in this study, we show these level diagrams in Figs. 1 (for g states) and 2 (for u states) because, so far, the level structure of strongly correlated high-lying vibrational excited states has seldom been visualized and these level distributions are, at the same time, our source of information for the following analysis. From these diagrams it is rather difficult to extract clear-cut information about the effect of classical chaos on the level structure. However, even at this stage, we notice a certain difference in level pattern across the high-energy region, particularly between $\delta = 0.01$ for a near-integrable case and $\delta = 0.31$ for a strongly coupled case. In particular, a number of rather wide energy gaps between two adjacent energy levels are observed more frequently for $\delta = 0.01$ than for $\delta = 0.31$. Since the number of energy levels is kept approximately constant ($\sim 410-430$) throughout all the δ values considered, this is interpreted as a manifestation of the so-called level-clustering phenomenon.[25] Before analyzing the mass ratio dependence of the Brody parameter, we show in Fig. 3 a staircase plot of the cumulative level number N and its unfolded version for g states, between $E = 0.5$ and 1.0 at $\delta = 0.30$. In the figure, the straight staircase plot has been unfolded by the transformation $E \rightarrow \tilde{E}$,[1,18]

$$\tilde{E} = b_1^{-1}(f(E) - b_0), \quad f(E) = \sum_{i=0}^{5} c_i E^i , \tag{19}$$

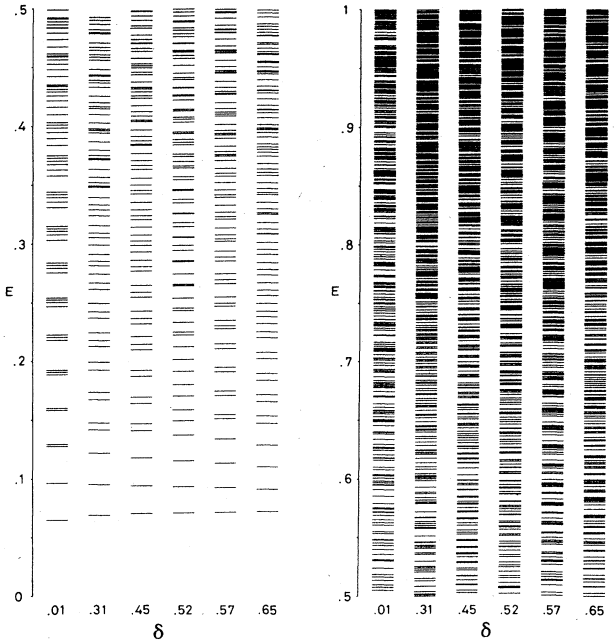

FIG. 1. Energy-level diagrams for g states at selected values of δ. Levels in the range $0 \leq E \leq 0.5$, which are not employed in the present analysis, are also shown for a comparison of the level spacing between low- and high-energy regions.

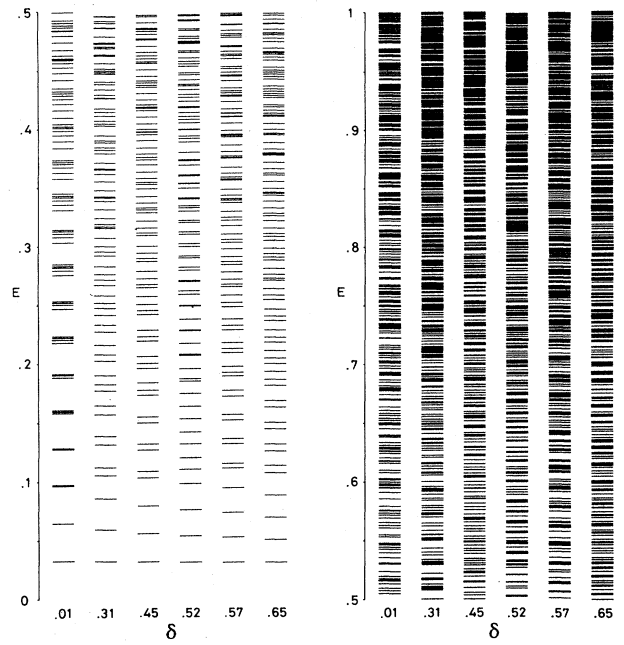

FIG. 2. Same as in Fig. 1 for u states.

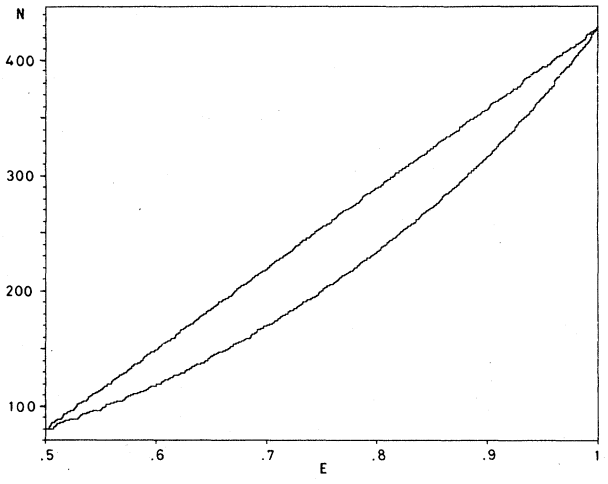

FIG. 3 Staircase plots of the cumulative level number as a function of energy for the range $0.5 \leq E \leq 1.0$ at $\delta = 0.30$. The plot lying on an arched curve is the original cumulative level number and that on a straight line the unfolded version obtained by the use of the relations Eqs. (19) in the text.

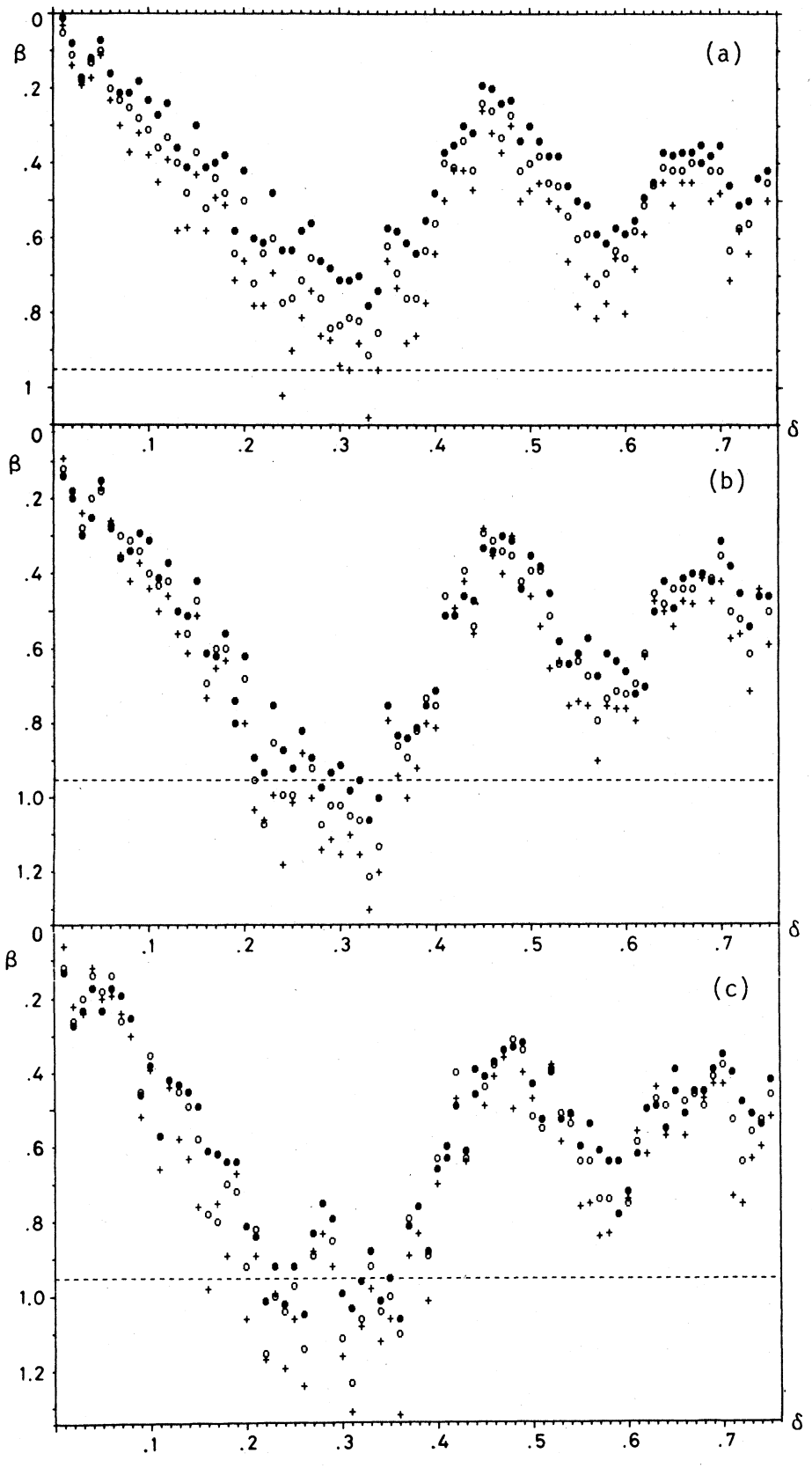

FIG. 4. Oscillatory patterns in the Brody parameter β vs mass ratio δ plots for (a) g states before unfolding, (b) g states after unfolding, and (c) u states after unfolding. In each figure, solid and open circles and crosses represent the three different energy ranges, $0.5 \leq E \leq 1.0$ (level number $N \sim 350$), $0.6 \leq E \leq 1.0$ ($N \sim 300$), and $0.7 \leq E \leq 1.0$ ($N \sim 250$), respectively, and the dashed line at $\beta = 0.953$ indicates the value of β corresponding to the Mehta-Gaudin distribution from the GOE. The plot for u states before unfolding is omitted because its relation to the unfolded version is essentially the same as that of (a) to (b).

where b_0 and b_1 are the intercept on the N axis and the slope, respectively, of the straight line connecting the two endpoints on the (E,N) plane, between which the unfolding is intended; f(E), a polynomial function of degree 5 being used for the smoothing of the original staircase plot of the cumulative level number, is determined by a least-squares fit.

Figures 4(a)—4(c) are plots of the Brody parameter β versus the modified mass ratio δ between $\delta=0.01$ and 0.75 for the three different energy ranges indicated. From the comparison of Figs. 4(a) and 4(b), which are for states with the same symmetry, we see that even before unfolding the overall oscillatory behavior of the Brody parameter is correctly described. This is considered primarily because of the fact that the level density over the energy ranges considered is fairly slowly varying as a function of energy, and in fact, as estimated approximately from Fig. 3, its rate of increase is about 10% between the two successive energy ranges indicated in Fig. 4. These plots (hereafter called the $\beta-\delta$ plots) should be compared to Fig. 1 in II, which is reproduced in Fig. 5. Oscillatory patterns in Fig. 4 correspond quite well to that in Fig. 5. A close look at these $\beta-\delta$ plots further reveals some remarkable features. The first is the location of δ values providing extrema of the plotted curves, which is regarded as a measure of the sharpness of the classical-quantum correspondence. From Figs. 4(a)—4(c) we observe that there are three minima around $\delta\cong 0.30$—0.33, 0.57—0.60, and 0.71—0.73, and two maxima around $\delta\cong 0.45$—0.49 and 0.65—0.70. Compared with Fig. 5, the shift of the positions of the δ values for these extrema toward larger values on the δ axis can immediately be noted. Detailed consideration of these shifts is provided in Sec. IV.

Another important point to be noted is the behavior of the parameter δ around the strong-coupling region, namely around the deepest valleys in the plots. Recent analyses of level-spacing distributions for billiard systems[13,14] strongly suggest that the distributions are sufficiently well represented by the Mehta-Gaudin distribution from the GOE. Accordingly, it is highly interesting and at the same time desirable to find out to what extent the quantum behavior of the present model system, which is classically not a K system, tends to that of the classical K system in the strong-coupling limit. As is easily noticed from Figs. 4(b) and 4(c), even after the unfolding procedure, it is not easy to decide on reliable values of β for the strong-coupling region because of the rather large statistical fluctuations in β values, introduced principally by the small number of energy levels employed. Consequently, we have examined the dependence of the Brody parameter on the magnitude of the level number, namely the manner of convergence of the parameter as a function of the level number N, between $N=110$ and 350.

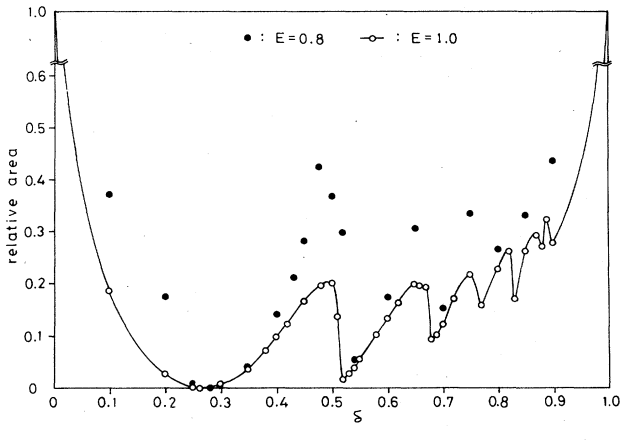

FIG. 5. Approximate relative areas of chaotic (and regular) regions to the entire surfaces of section on the $(\hat{p}_1,q_1)$ plane as a function of the mass ratio δ [redrawn from Fig. 1 in II (Ref. 21)]. The upper regions above the solid curve for $E=1.0$ and the solid circles for $E=0.8$ correspond to the relative areas of chaotic regions for the respective energies. Compared with Fig. 1 in II, for $E=0.8$, three additional data are supplied for further details between $\delta=0.4$ and 0.5.

Figure 6 shows some results of this convergence check conducted for $\delta=0.30$. From the figure, we see that convergence is not rapid and even at $N\cong 300$ the fluctuation width $\Delta\beta$ is estimated as $\Delta\beta\cong\pm 0.15$. However, from the behavior of the fluctuation curves, the parameter may be expected to settle at a convergent value somewhere between $\beta=0.953$ from the GOE and $\beta=1.1$, an estimated upper bound. This conjecture leads to the important conclusion that a Hamilton system without a classical K-system property could not be distinguished quantum mechanically from a complete K system. This consequence, however, is not particularly unexpected, because in the quantum-mechanical limit the concept of trajectory in phase space is no longer valid as a result of the so-called coarse graining of the phase space. In this sense the present result raises an interesting question about how useful or how necessary the definition of the term "quantum K system"[8] is. The result of Fig. 6 also suggests that, according to the $1/\sqrt{N}$ fluctuation law in statistics, at least about 40 000 energy levels are necessary to reduce the fluctuation width to one-tenth of the present level, which is sufficient to make a clearer correspondence between classical and quantum systems. At the present stage, however, it is almost hopeless to diagonalize such a huge dimensional matrix to a sufficient degree of accuracy. Since triatomic systems would be unlikely to have such a great number of vibrational energy levels below the dissociation threshold, it will be difficult to find a clearer manifestation of classical-quantum correspondence for triatomic systems, unless the rotational degrees of freedom are incorporated at the same time.

Figures 7(a) and 7(b) show some typical distribution curves selected mostley from those corresponding to extremal points on the $\beta-\delta$ curves in Fig. 4. These figures actually constitute extended and refined versions of those reported in Fig. 4 in I, and qualitative conclusions stated there concerning the positions of maxima in histograms have now been quantified by the use of parameter β. As seen from the curve profiles for $\delta=0.01$ and 0.05, the prediction that the distribution tends to the Poisson type in the integrable or near-integrable limit is again confirmed in the present analysis. This result further tells us

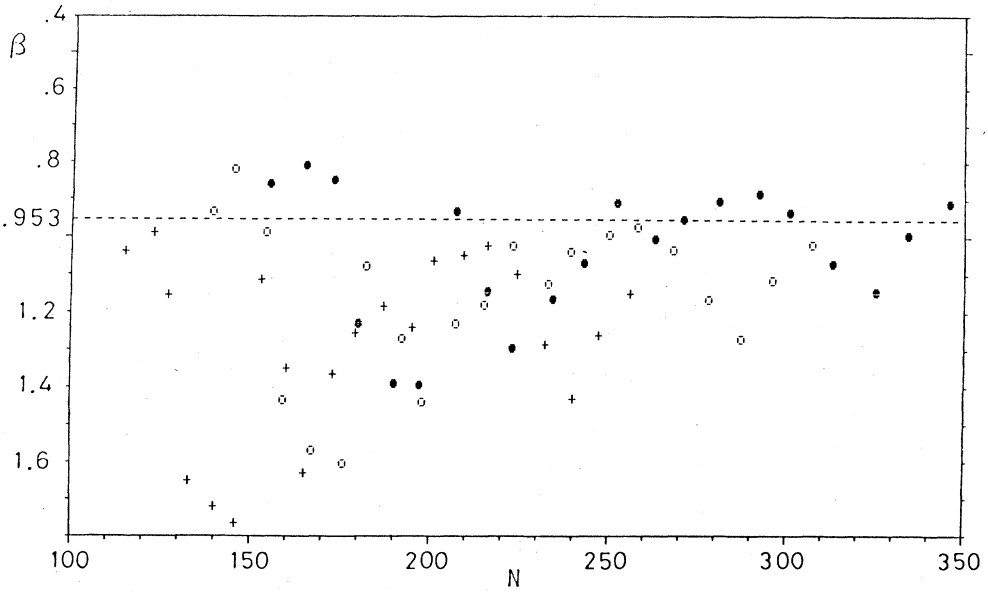

FIG. 6. Statistical fluctuations of the Brody parameter as a function of the level number N at $\delta=0.30$. The three different plots correspond to the three different energy ranges denoted by the same symbols as in Fig. 4.

that the information obtained from the profiles of the distribution curves could provide a useful means for measuring the degree of the mode coupling and for predicting or detecting a local mode in the system. Spectroscopically this will be quite useful, although it would be highly difficult to construct, from experimental observations, a spacing distribution consisting solely of energy levels with the same symmetry class.

In concluding this section we would like to mention the behavior of the Brody parameter in the interval $0.75 \leq \delta \leq 1.0$, over which we have not extended our analysis in the present paper. Judging from both the trend in Fig. 4 and the classical results in II, we expect that the oscillatory patterns in the $\beta-\delta$ plots become gradually more obscure as δ is increased and the spacing distribution again tends to the Poisson type.

IV. COMPARISON WITH CLASSICAL RESULTS

In this section we explore is some detail the relationship between the oscillatory behavior observed in Fig. 4 in the preceding section and the changes in the approximate area ratios of the chaotic and regular regions on the Poincaré surfaces of section in the corresponding classical systems.

Figures 8 and 9 show the mass ratio δ dependence of the Poincaré sections at both selected δ values (which correspond mostly to extremal β values) and energy values, $E=0.5$, 0.6, 0.7, and 0.9. Of these energy values, the first three are those of the lower bounds in the three energy ranges treated in Fig. 4. The δ dependence of both regular-chaotic area ratios and the geometrical patterns of the persisting central islands at $E=1.0$ is only referred to as required, because those results have already been reported in II. From an overview of these figures the following general features are extracted. Firstly, by following up the patterns in increasing order of δ at each energy value except $E=0.5$, one can notice the oscillatory patterns in the size of the chaotic (or regular) regions (including those of higher-order islands surrounding the central one), although the positions of the δ values providing the minimum or maximum island size vary from energy to energy. At $E=0.5$ there is no large-scale chaos observed, except for $\delta=0.26$ and 0.31 for which fairly well-developed chaotic regions are visible near the boundaries of the surfaces of section. Secondly, although the size of the islands generally decreases with increasing energy, there are certain exceptions; namely, at $\delta=0.31$ there occurs a reversion in island size between $E=0.6$ and 0.9, and at $\delta=0.57$ the size of islands is almost the same between $E=0.7$ and 0.9.

We now proceed to elucidate these features in some detail. As already noted in the preceding section in connection with the relationship between Figs. 4 and 5, when $E=1.0$, the position of δ giving the smallest island (actually its area converges to a point) is found at $\delta \cong 0.263$ and the next smallest island at $\delta \cong 0.508$, in contrast to the corresponding minima in Fig. 4 found at $\delta \cong 0.30$—0.33 and 0.57, respectively. In II we mentioned the general trend that the position of the δ value providing the third-order resonance point[26] moves in the negative δ direction on the δ axis as the energy increases. In order to confirm this trend we have further explored the variation of δ giving both third- and fourth- order resonance points (actually the latter is a combination of two second-order resonances as stated in II) in the (δ,E) parameter plane. Presented in Fig. 11 and supplemented with Fig. 10 is the result of the follow up of these moves on the (δ,E) plane. The third-order resonance point represented by the separatrix, Fig. 10.2, at the center of which the point is located starts at $\delta=0.384$, which can be calculated from the expression giving the winding number in the $E \rightarrow 0$ limit:[21]

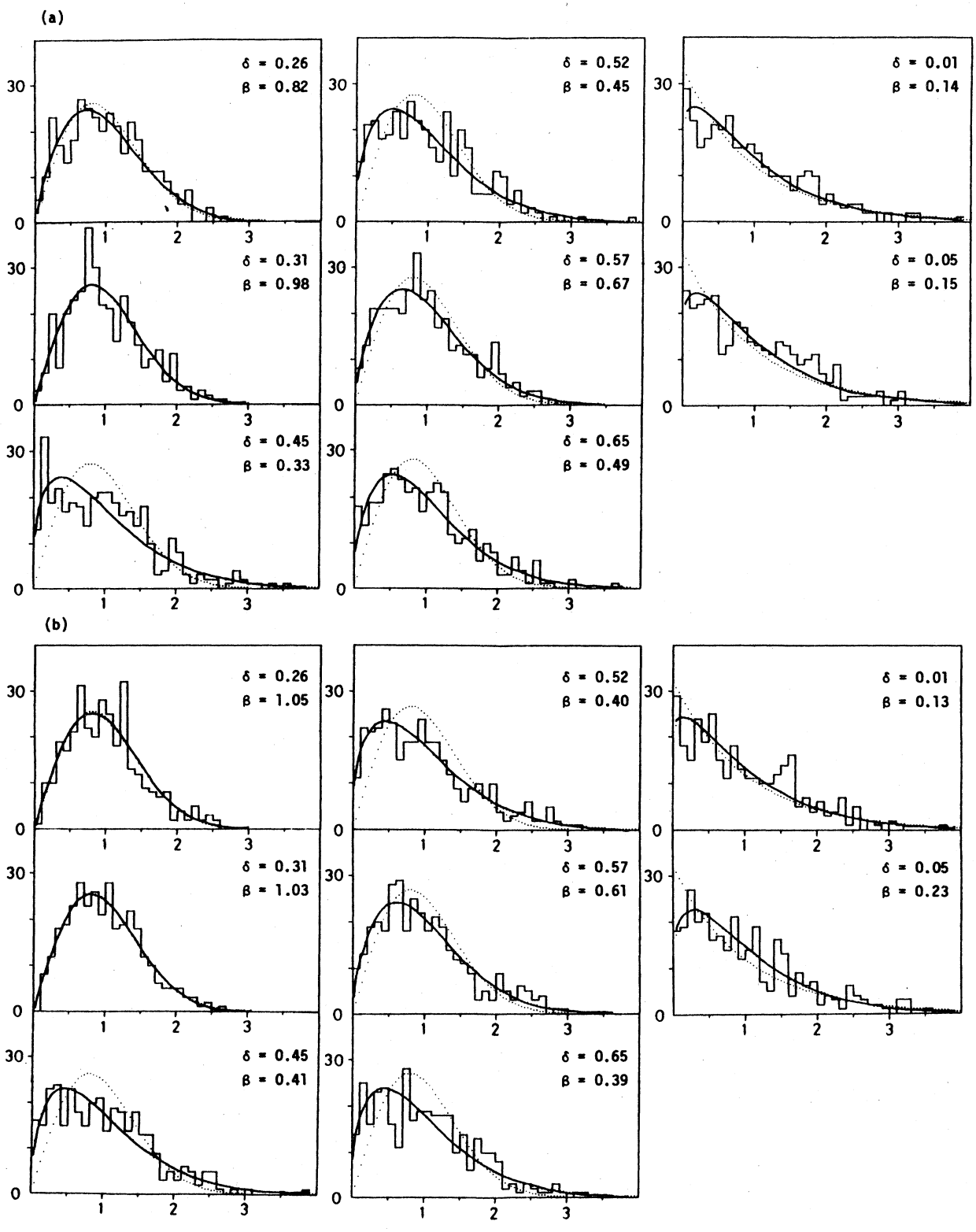

FIG. 7. Nearest-neighbor level-spacing distributions for (a) g states and (b) u states at typical δ values selected from Figs. 4(b) and 4(c). In the left-hand and middle columns, the dotted curves correspond to the Mehta-Gaudin distributions and those in the right-hand column to the Poisson distributions. For all figures, the vertical axes represent the number of spacings and the horizontal axes the normalized mean spacing z $(=s/\bar{s})$.

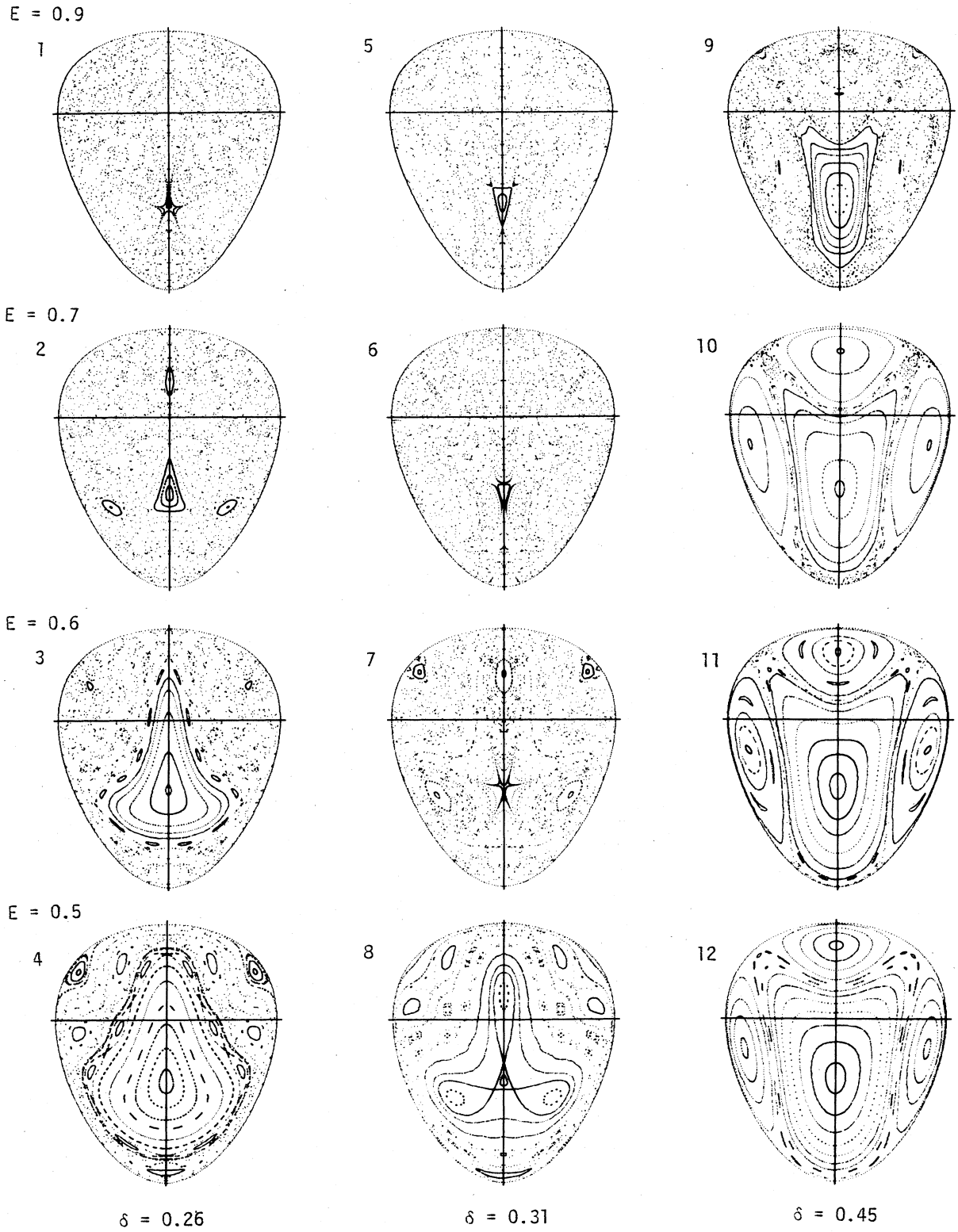

FIG. 8. Poincaré surfaces of section at several selected points on the (δ, E) parameter plane. For all figures, vertical axes represent symmetric stretching normal coordinates (q_1 in II) and horizontal axes their conjugate momenta ($\hat{p}_1$ in II). Scales of all the coordinate axes are appropriately adjusted so that all the figures have approximately the same size.

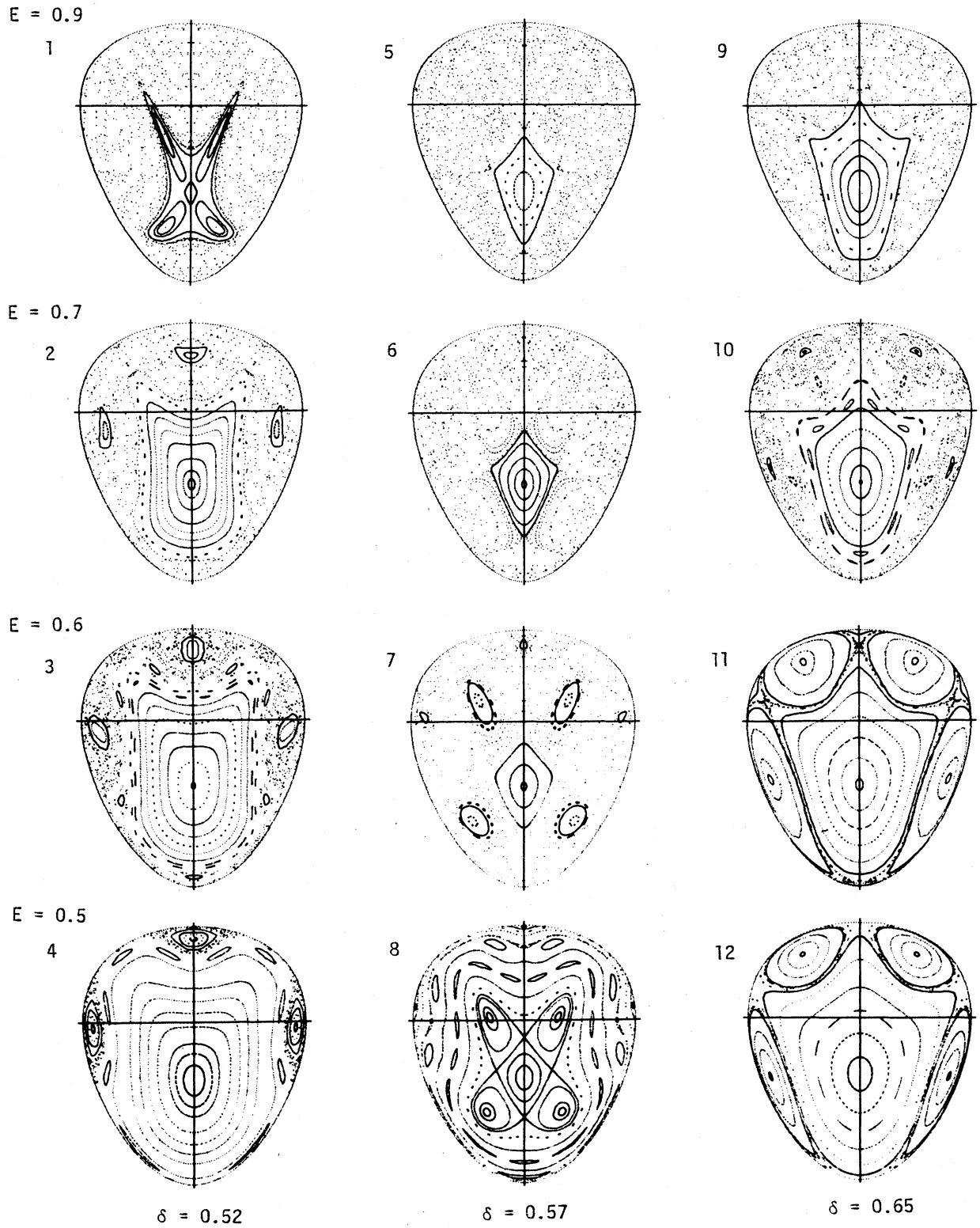

FIG. 9. Same as Fig. 8 for $\delta=0.52$, 0.57, and 0.65.

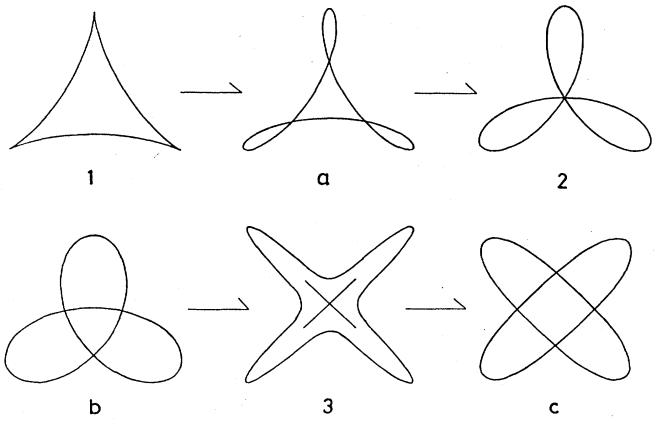

FIG. 10. Topological patterns of typical separatrices appearing in accordance with the increase in δ. Separatrices designated by 1, 2, and 3 form the lines represented by the corresponding numbers on the (δ,E) plane, as shown in Fig. 11. Separatrices a, b, and c also occupy certain domains on the same parameter plane as also indicated in Fig. 11.

$$\omega_1/\omega_2=[\gamma/(\gamma+2)]^{1/2},\quad \delta=(1+\gamma)^{-1} \tag{20}$$

by setting $\omega_1/\omega_2=\frac{2}{3}$. Then the point shifts gradually in the negative δ direction and arrives at $\delta\cong 0.263$ at $E=1.0$. The fourth-order resonance case characterized by the separatrix, Fig. 10.3, proceeds similarly, starting at $\delta=0.60$ [which is also calculated from Eq. (20) by setting $\omega_1/\omega_2=\frac{1}{2}$] and arriving at $\delta\cong 0.508$ at $E=1.0$.

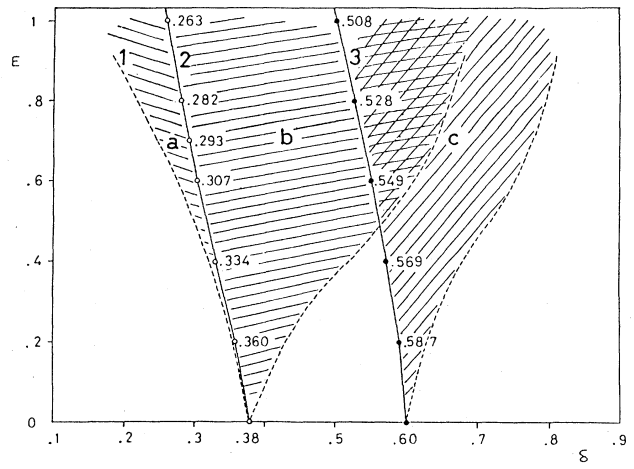

FIG. 11. Movements of the third- and fourth-order resonance points on the (δ,E) parameter plane. In the figure, lines indicated by 1, 2, and 3 correspond to the separatrices designated by the same numbers in Fig. 10 and three different shaded areas indicated by a, b, and c also correspond to separatrices with the same designation in Fig. 10. In the doubly hatched intersection of b and c, the separatrix c (and, accordingly, four periodic points) lies inside the separatrix b, that is inside the three periodic points. Dotted lines, except line 1, indicate the positions on the parameter plane at which three or four periodic points are absorbed into the boundaries of mapping planes.

From Figs. 10 and 11 we can now understand the general behavior of the geometrical patterns appearing on the surfaces of section in Figs. 8 and 9. Namely, in Fig. 10 we see that the apex of the triangle-shaped island inside the separatrix is upward (Fig. 10a) or downward (Fig. 10b) according to whether the separatrix is below or above line 2 (Fig. 11). This situation is actually observed in pictures for $\delta=0.26$ and 0.31, for example, in Figs. 8.2 and 8.6 or in Figs. 8.6 and 8.8. The similar situation, in which four periodic points are generated above line 3 (Fig. 11), is also expected for the fourth-order resonance case, and island patterns just after the occurrence of such a bifurcation are, in fact, seen in Figs. 9.1, 9.7, and 9.8. It has been known that for nonintegrable systems the stochastic layers or homoclinic tangles centering around the hyperbolic fixed points always exist along the separatrices, and, generally with increasing perturbation strength, these layers develop gradually to form a large-scale or global chaotic region by the resonance overlap. This means in Fig. 11 that the region with most developed chaos on both sides of line 2 (we call the region the "third-order resonance zone") moves toward the left-hand side on the (δ,E) plane, in accordance with the leftward shift of the third-order resonance point represented in Fig. 10.2. The fourth-order case goes in much the same way. However, it is noted in this case that there is no chaotic development on the left-hand side of line 3 because, in the bifurcation from Fig. 10.3 to Fig. 10c, four hyperbolic fixed points turn out to be generated from the origin (the center of the two crossed lines in Fig. 10.3), and its bifurcation mechanism is thought to be the same as that of the one-parameter quadratic map on the plane analyzed by Henon.[27]

From the above considerations we can also understand quite naturally the reason for the reversion in island size, i.e., the increase in island area with energy, observed from Figs. 8.7 to 8.5. In particular, we see that Fig. 8.7 represents nothing other than the passage of the third-order resonance point corresponding to Fig. 10.2. Since Fig. 8.6 is closer to the resonance point lying on line 2 than Fig. 8.5, it is expected that Fig. 8.5 will have a larger island than Fig. 8.6 However, it should also be noted that the islands tend, generally with increasing energy, to be gradually eroded under the influence of the surrounding chaotic trajectories, and this is seen in almost all pictures in Figs. 8 and 9 expect a few. Therefore, the case of Figs. 9.5 and 9.6 is thought to be a result of the balance between the increase and the erosion of the islands. Concerning this, we point out that along these resonance zones there is a general possibility of the occurrence of such a reversion in island size, i.e., a kind of island oscillation with energy, and actually we observe such cases far beyond the dissociation threshold at certain δ values.[28]

We now turn to the question raised in the preceding section of why the minima in the $\beta-\delta$ plots in Fig. 4 are located around $\delta\cong 0.31-0.33$, shifted to the right from the value of $\delta\cong 0.263$. As stated in I, nearest-neighbor level-spacing distributions now under study cover a fairly wide range of energies extending from $E=0.5$ to 1.0. Accordingly, it is obvious that there is no one-to-one correspondence between a level-spacing distribution and a

particular Poincaré map defined and drawn for a certian fixed energy value. This implies that a level-spacing distribution constructed for a particular energy interval at a particular δ should be linked to the behavior of an averaged pattern taken over all the Poincaré maps involved in that energy interval. By making this correspondence, we can satisfactorily explain the oscillatory pattern appearing in Fig. 4. For example, by comparing pictures of Figs. 8.1—8.4 for $\delta=0.26$ with those of Figs. 8.5—8.8 for $\delta=0.31$, we see that the Brody parameters for $\delta=0.31$ should generally take larger values than those for $\delta=0.26$ since there still persist fairly large islands on the Poincaré maps at lower energies (Figs. 8.3 and 8.4) for the latter δ value. For $\delta=0.45$ and, in part, for $\delta=0.52$, at which there occurs no passage of the resonance zones, fairly large islands persist up to higher energies. This naturally contributes to the formation of the peak in the $\beta-\delta$ plots around $\delta\cong 0.45$—0.50. Similar arguments are applicable to a lesser extent to the cases of the peak and valley found at $\delta\cong 0.65$ and 0.57, respectively. Thus, we can see that the location of the low-order resonance zone on the (δ,E) parameter space plays an essential role in generating global chaos.

At this point we now consider how the above qualitative argument about the classical-quantum correspondence could further be quantified. This could, in principle, be achieved by finding (i) a method for taking a unique average of the fractions of chaotic (or regular) regions in Poincaré sections over a specified energy range, and (ii) an analytical relationship between the parameter β and the averaged fraction of chaotic regions in Poincaré sections. We believe that these two things could be carried out at least for relatively small energy ranges over which there are no drastic and complicated changes in the fraction of chaotic regions. For the present system, however, as seen in Figs. 8 and 9, the fraction of chaotic or regular regions in a Poincaré section changes rather widely over the energy range $0.5\leq E\leq 1.0$, in which only about 350 energy levels are contained. Thus, at the moment, the general pursuit of this problem is exceedingly difficult.

Concerning this classical-quantum correspondence problem, it is highly interesting to make some comparison of the present result with those obtained by use of the Berry-Robnik distribution[24] recently proposed for the semiclassical limit:

$$P_\rho(z)=\frac{d^2}{dz^2}\{\exp[(\rho-1)z]\mathrm{erfc}(\sqrt{\pi}\rho z/2)\}\ , \tag{21}$$

with

$$\mathrm{erfc}(x)=(2/\sqrt{\pi})\int_x^\infty \exp(-t^2)dt\ ,$$

where ρ is the fraction of the chaotic region on the Poincaré section at a given energy with a sufficiently small energy interval ΔE, and the variable z is the same as defined in Eq. (17). Our interest here is to see what result is obtained by reinterpreting the parameter ρ in Eq. (21) as an effective fraction averaged over a specified energy range, not as that of a particular energy.

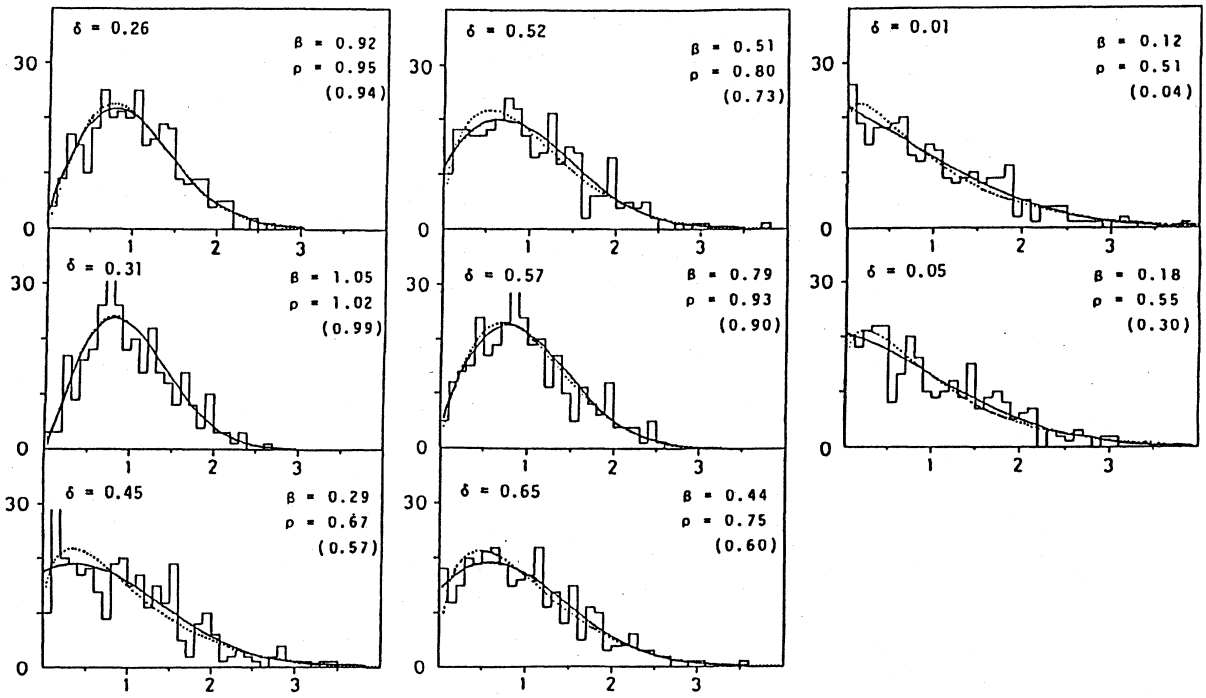

FIG. 12. Comparison of the Brody and Berry-Robnik distributions for g states in the energy range $0.6\leq E\leq 1.0$. The solid curves represent Berry-Robnik distributions, whose parameters ρ are determined by the least-squares fit to the given histograms, and the dotted curves are Brody distributions obtained by the same procedure from the corresponding histograms. The values of ρ indicated in parentheses are those obtained directly from the Poincaré sections by taking an average of five different fractions of chaotic regions at $E=$ 0.6, 0.7, 0.8, 0.9, and 1.0.

Figure 12 shows a comparison of the Brody and Berry-Robnik distribution curves for the same histograms as in Fig. 7(a). The values of ρ for these distribution curves have been determined by a nonlinear least-squares fit to the given histograms in the figures. From these figures we observe that for strong- or quasistrong-coupling cases ($\delta=0.26$, 0.31, and 0.57) the three parameters—β and ρ obtained from the Berry-Robnik distributions and the parameter ρ obtained directly from the Poincaré sections by averaging the fractions of chaotic regions—give almost the same values. However, as coupling is decreased these parameters begin gradually to take their own values independently of each other. Of these three parameters, the one showing the most rapid change with the variation of δ is β, and its sensitivity to the change in δ is surely a favorable factor in using this as an indicator for measuring the degree of mode coupling, while its distribution curve has a sharper curvature around its maximum region than the Berry-Robnik distribution, which is much broader in its curve profile around the corresponding region. As is shown in the value of ρ in Fig. 12, a remarkable feature of the Berry-Robnik distribution is the large deviation of its parameter ρ from that obtained by the averaging in regions where δ is small. In particular, at $\delta=0.01$, which corresponds to a near-integrable case, the value $\rho=0.51$ obtained from the least-squares fit to the histogram makes a striking contrast to the value $\rho=0.04$ obtained by the average of five different fractions of chaotic regions at indicated energies. It might be possible that this discrepancy in the two ρ values in near-integrable regions is caused by a quantum effect, i.e., an insufficiently small finite $\hbar$, but detailed analysis of this discrepancy remains to be done. Thus, it has turned out that except for strong-coupling regions we cannot give a simple interpretation to the values of ρ from the Berry-Robnik distribution as an averaged fraction of chaotic regions over the specified energy interval, although we can, of course, use it as an adjustable parameter for measuring the degree of chaos.

Finally in concluding this section, we note that, as also stated in II, the changes in mapping behavior as a function of mass ratio δ is very close to that in the Henon map, except for regions where δ is small. This implies that mass ratio performs a greater part of the role played by the rotation angle in the Henon map, for certain energy ranges.

V. SUMMARY AND CONCLUDING REMARKS

In this paper we have explored the relationship between the degree of classical chaos and the behavior manifested in the quantum level-spacing distributions and attempted to quantify that relationship in terms of the Brody parameter characterizing the strength of the level repulsion. We found a fairly good correspondence between the oscillatory patterns in approximate fractions of chaotic regions on Poincaré sections and those in the mass ratio dependence of the Brody parameter. Furthermore, the origin of oscillatory patterns is investigated in some detail and it is elucidated that low-order (namely, third- and fourth-order) resonance zones shift very slowly toward smaller values of δ as energy increases, i.e., they are slowly varying functions of energy. Stated another way, they are almost independent of energy and this fact, in turn, ensures the classical-quantum correspondence at approximately the same δ values despite the fact that there is no one-to-one correspondence between a particular quantum energy spectrum and a Poincaré map drawn at a particular fixed energy. Another remarkable result obtained in this study is that, throughout the strong-coupling region with mass ratio $\delta=0.3$—0.35 the behavior of level-spacing distributions for the present model system is not distinguishable from that of quantum level-spacing distributions for the classical K system. This would quite reasonably be expected as a result of the quantum-mechanical coarse graning of phase space, as stated in Sec. III.

In the present study, the Brody parameter has been shown to be quite convenient and useful in extracting a greater part of the magnitude of mode coupling. However, as mentioned at the end of Sec. II, the Brody distribution has been devised empirically to connect the Wigner distribution with the Poisson distribution, and it should be interpreted as a practical, effective distribution. Since, at present, applications of the Berry-Robnik distribution to general cases with a wide energy range like the present one are considered highly difficult,[24] we will have to admit the practical usefulness of the Brody distribution (and its parameter), as long as it turns out to incorporate a greater and essential part of the mode coupling. In order to clarify both the validity and the limitations of its applicability, therefore, its application to a wider class of systems[29] is both desirable and necessary. Also, exploring a possible numerical relationship between the Brody and Berry-Robnik distributions for feasible cases would be useful.

Finally, it should also be noted that the Wigner (or more precisely, Mehta-Gaudin) distribution is based on the GOE. As is well known, the statistical independence between the matrix elements, one of the two fundamental assumptions in the GOE, is a postulate not based on a physical principle or insight but on the necessity of mathematical tractability, and the possible choice of the weight function in the probability density is very wide. Consequently, there remains the problem of exploring a probability distribution function that more faithfully reflects the characteristics of the Hamiltonian of the system, although it will be not an easy task to perform. It is, of course, expected or highly likely that statistics calculated by the use of such a distribution as derived from physically well-founded constraints will give approximately the same results as those from the GOE. Then, a statistic based on the GOE will for the first time attain an established position as a useful first approximation to the true ensemble average derived from a physically more plausible ensemble.

ACKNOWLEDGMENT

One of us (T. M.) is grateful to Professor S. Iwata for his continual interest and encouragement in the course of this work.

[1]T. A. Brody, J. Flores, J. B. French, P. A. Mello, A. Pandey, and S. S. M. Wong, Rev. Mod Phys. **53**, 385 (1981), and references therein.
[2]C. E. Porter, *Statistical Theories of Spectra: Fluctuations* (Academic, New York, 1965).
[3]E. P. Wigner, SIAM Rev. **9**, 1 (1967).
[4]M. L. Mehta, *Random Matrices and the Statistical Theory of Energy Levels* (Academic, New York, 1967).
[5]S. W. McDonald and A. N. Kaufman, Phys. Rev. Lett. **42**, 1189 (1979).
[6]G. Casati, F. Valz-Gris, and I. Guarneri, Lett. Nuovo Cimento **28**, 279 (1980).
[7]M. V. Berry, Ann. Phys. (N. Y.) **131**, 163 (1981).
[8]G. M. Zaslavsky, Phys. Rep. **80**, 157 (1981).
[9]V. Buch, R. B. Gerber, and M. A. Ratner, J. Chem. Phys. **76**, 5397 (1982).
[10]P. Pechukas, Phys. Rev. Lett **51**, 943 (1983).
[11]A. J. Lichtenberg and M. A. Lieberman, *Regular and Stochastic Motion* (Springer New York, 1983), Appendix A.6.
[12]T. Matsushita and T. Terasaka, Chem. Phys. Lett. **105**, 511 (1984).
[13]O. Bohigas, M. J. Giannoni, and C. Schmit, Phys. Rev. Lett **52**, 1 (1984).
[14]O. Bohigas and M. J. Giannoni, *Chaotic Motion and Random Matrix Theories,* Vol. 209 of *Lecture Notes in Physics, Mathematical and Computational Methods in Nuclear Physics* (Springer, Berlin, in press).
[15]M. L. Mehta, Nucl. Phys. **18**, 395 (1960).
[16]M. Gaudin, Nucl. Phys. **25**, 447 (1961).
[17]J. Chaiken, M. Gurnik, and J. D. McDonald, J. Chem. Phys. **74**, 117 (1981).
[18]E. Haller, H. Koppel, and L. S. Cederbaum, Chem. Phys. Lett. **101**, 215 (1983).
[19]S. Mukamel, J. Sue, and A. Pandey, Chem. Phys. Lett. **105**, 134 (1984).
[20]E. Abramson, R. W. Field, D. Imre, K. K. Innes, and J. L. Kinsey, J. Chem. Phys. **80** 2298 (1984).
[21]T. Matsushita and T. Terasaka, Chem. Phys. Lett. **100**, 138 (1983).
[22]T. A. Brody, Lett. Nuovo Cimento **7**, 482 (1973).
[23]See also W. E. Smyser and D. J. Wilson, J. Chem. Phys. **50**, 182 (1969); M. L. Sage, Chem. Phys. **35**, 375 (1978).
[24]As one of such distribution functions, recently Berry and Robnik [M. V. Berry and M. Robnik, J. Phys. A **17**, 2413 (1984)] introduced a semiclassical level-spacing distribution interpolating between the Poisson and Wigner distributions in the semiclassical limit.
[25]M. V. Berry, Philos. Trans. R. Soc. London, Ser. A **287**, 237 (1977); J. Phys. A **10**, 2083 (1977).
[26]Throughout this article, by the third-order "resonance point" we mean the center or self-intersecting triple point of the separatrix represented by Fig. 10.2. For the same type of the point, see, for example, V. I. Arnold, *Mathmetical Methods of Classical Mechanics* (Springer, New York, 1978), p. 392.
[27]M. Henon, Quart. Appl. Math. **27**, 291 (1969).
[28]T. Matsushita and T. Terasaka (unpublished).
[29]The two very recent papers for other simpler model systems we noticed after the completion of the present analysis, M. Robnik, J. Phys. A **17**, 1049 (1984) and E. Haller, H. Köppel, and L. S. Cederbaum, Phys. Rev. Lett. **52**, 1665 (1984), seem to obtain similar conclusions to those in this and our previous (Ref. 12) articles.